THE ASTROPHYSICAL JOURNAL, 493:970–977, 1998 February 1

EARLY EVOLUTION OF CORONAL ACTIVE REGIONS OBSERVED WITH THE *YOHKOH* SOFT X-RAY TELESCOPE. I. EXPANSION VELOCITY

SEIJI YASHIRO,[1] KAZUNARI SHIBATA,[2] AND MASUMI SHIMOJO[3]
Received 1996 July 5; accepted 1997 September 10

ABSTRACT

We study the early evolution of active regions in the corona by analyzing 33 emerging flux regions (EFRs) observed with the soft X-ray telescope (SXT) aboard *Yohkoh* during the period from 1992 February to 1996 May. We examine the time variation of the size (projected area) and the total soft X-ray intensity of the EFRs, and find that the time-averaged apparent velocity of the expansion of most of the EFRs is less than 2 km s^{-1} during the very early phase ($t < 6$–14 hr after the birth of the EFRs). The average expansion velocity of 33 EFRs is 1.5 km s^{-1}. This expansion velocity is much lower than the rise velocity of emerging magnetic loop in the upper chromosphere, inferred from Hα observations of arch filament systems as well as MHD simulation and theory. Some possibilities to account for this discrepancy are discussed.

Subject headings: Sun: activity — Sun: corona — Sun: magnetic fields — Sun: X-rays, gamma rays

1. INTRODUCTION

Newly emerged solar active regions (ARs) are referred to as emerging flux regions (EFRs) (Zirin 1972). EFRs are one of the key phenomena for understanding solar activity and the origin of solar magnetic fields. Dynamic phenomena such as jets and microflares have often been observed in EFRs (Marsh 1978; Kurokawa 1988; Yokoyama & Shibata 1995, 1996; Shibata, Yokoyama, & Shimojo 1996; Shimojo et al. 1996; Shimizu et al. 1996), and even intense flares are often driven by EFRs (Zirin 1988; Gaizauskas 1993). Emerging magnetic flux is thought to be originally formed by the dynamo action in the deep interior of the Sun and carried to the surface by the magnetic buoyancy (Parker 1979; Zwaan 1987), and so it can be used to study magnetic fields below the surface (and ultimately the dynamo process).

In the chromosphere, EFRs are seen as arch filament systems (AFSs) in Hα (Bruzek 1967, 1969; Zwaan 1987; Gaizauskas 1993) and have been studied extensively. It is known that the rise velocity of arch filaments (=emerging magnetic loops in the upper chromosphere) is ~10–20 km s^{-1} (Bruzek 1969; Chou & Zirin 1988). Shibata et al. (1989) performed the two-dimensional magnetohydrodynamic (MHD) numerical simulations of emerging flux in the photosphere/chromosphere and the low corona, and obtained results consistent with Hα observations.

The properties of EFRs in the corona, however, have not been studied well, since the spatial and temporal resolution of previous soft X-ray observations was not adequate for a detailed study of EFRs (see Webb 1981 for a review of studies of coronal EFRs during the *Skylab* era).

The soft X-ray telescope (SXT) (Tsuneta et al. 1991) aboard *Yohkoh* (Ogawara et al. 1991) has provided us with the first opportunity to observe emerging flux regions in the corona for extended time periods (several days) with high spatial and temporal resolution.

Until now, several studies have been made on EFRs in the corona using *Yohkoh* data (Ishido et al. 1992; Kawai et al. 1992; Su et al. 1995). To date, however, EFR studies using SXT data were either preliminary (Ishido et al. 1992; Su et al. 1995) or very specific (see Kawai et al. 1992, who made detailed comparisons between Hα and soft X-ray images but did not study the evolution of EFRs). Although little is known about the evolution of coronal EFRs, no one has yet studied it in a systematic way using *Yohkoh* data

In this paper we present initial results of a systematic study of EFR evolution in the solar corona. It should be noted here that ground-based observations show that the *horizontal* expansion velocity of active regions or the separation velocity of two bipoles in active regions is a few kilometers per second in the early phase of their evolution (e.g., Chou 1993). However, we are particularly interested in the *vertical* expansion velocity of active regions, because it is related to the energy flux transported by emerging flux into the corona (i.e., Poynting flux $\simeq vB^2/4\pi \simeq 10^8(v/10$ km $s^{-1})(B/30\mathrm{G})^2$ ergs cm^{-2} s^{-1}, where v is the expansion velocity of emerging flux and B is the magnetic field strength). It is not known what the *vertical* expansion velocity of ARs is. Hα observations show that the rise velocity of emerging flux in the upper chromosphere is about 10 km s^{-1}, much larger than the horizontal expansion velocity. Since plasmas are frozen to magnetic field, this suggests that the vertical expansion velocity of EFRs just above arch filaments may be about 10 km s^{-1}. It is our primary purpose to examine this vertical expansion velocity in the *corona* high above arch filaments. Although it is not easy to measure the vertical expansion velocity, we note that the coronal EFRs generally show three-dimensional structure, more like a hemisphere than a plane, suggesting that at least the *apparent vertical* expansion velocity could be measured from the *apparent projected* (*or horizontal*) expansion velocity of EFRs. Hence we measure the apparent projected expansion velocity of EFRs in detail in this paper. In § 2 the method of observation and analysis is described. The results of measurement of the apparent expansion velocity of a typical EFR (NOAA 7732) and those of 33 EFRs are presented in § 3 with some description of the morphological evolution of NOAA 7732. We found that the initial apparent expansion velocity of most of the coronal EFRs is 0.2–2.5 km s^{-1},

[1] Department of Astronomy, School of Science, University of Tokyo, Hongo, Bunkyo, Tokyo 113, Japan.
[2] National Astronomical Observatory of Japan, 2-21-1, Osawa, Mitaka, Tokyo 181, Japan.
[3] Department of Astronomical Science, Graduate University for Advanced Studies, National Astronomical Observatory of Japan, 2-21-1, Osawa, Mitaka, Tokyo 181, Japan.

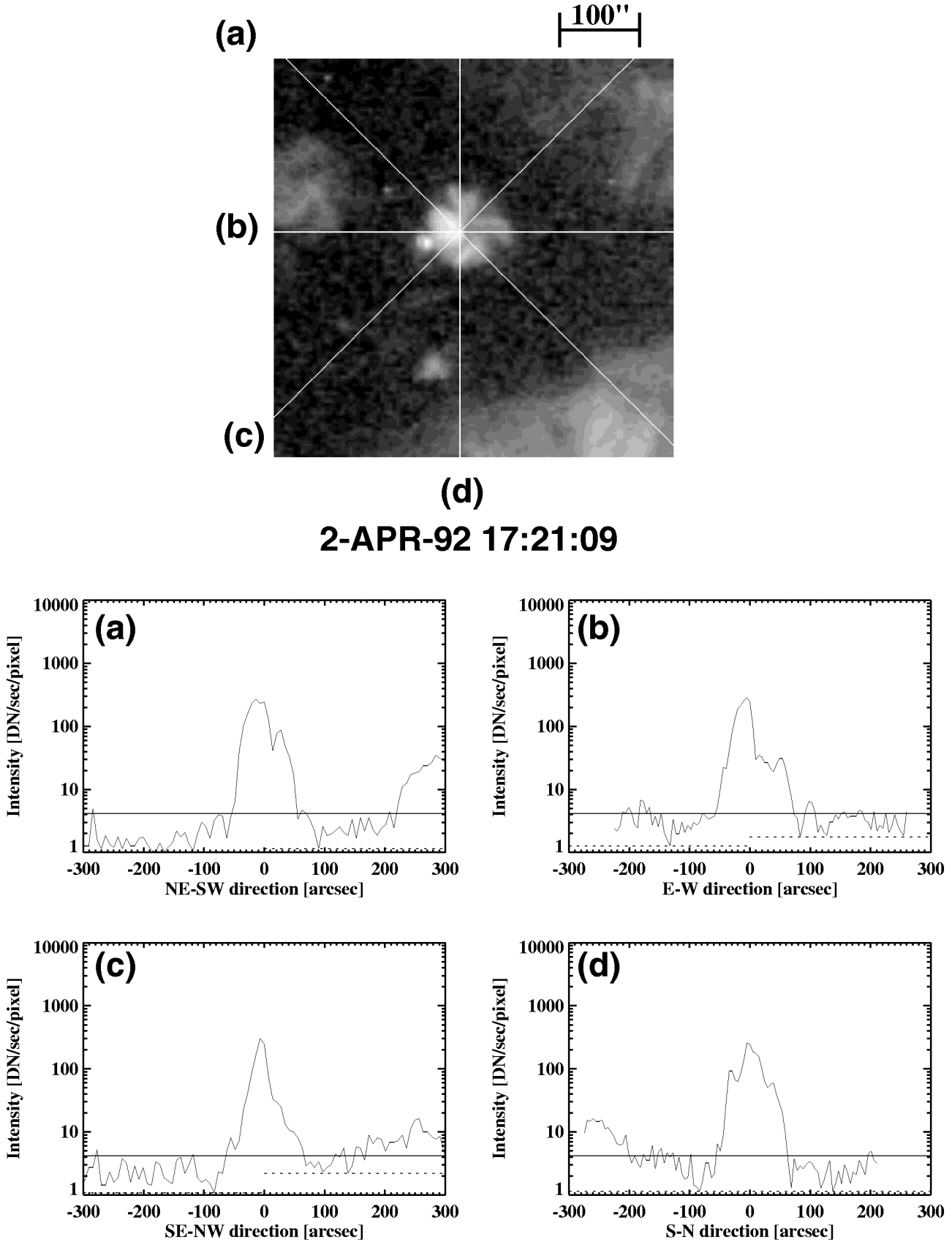

FIG. 1.—*Upper panel*: Soft X-ray (SXR) image of AR 7124 on 1992 April 2 at 17:21:09 UT. In the image, north is at the top and west is to the right. *Lower panels*: Panels (*a*)–(*d*) show the X-ray intensity distribution along the four straight lines (*a*)–(*d*), respectively, in the SXR image in the upper panel. The dashed lines show the minimum value of the X-ray intensity along each line on either side of the active region. Note that the maximum of these minimum values is less than 5 DN s^{-1} $pixel^{-1}$. Hence the 5 DN s^{-1} $pixel^{-1}$ level (denoted by the solid line) is defined as the boundary value of the active region.

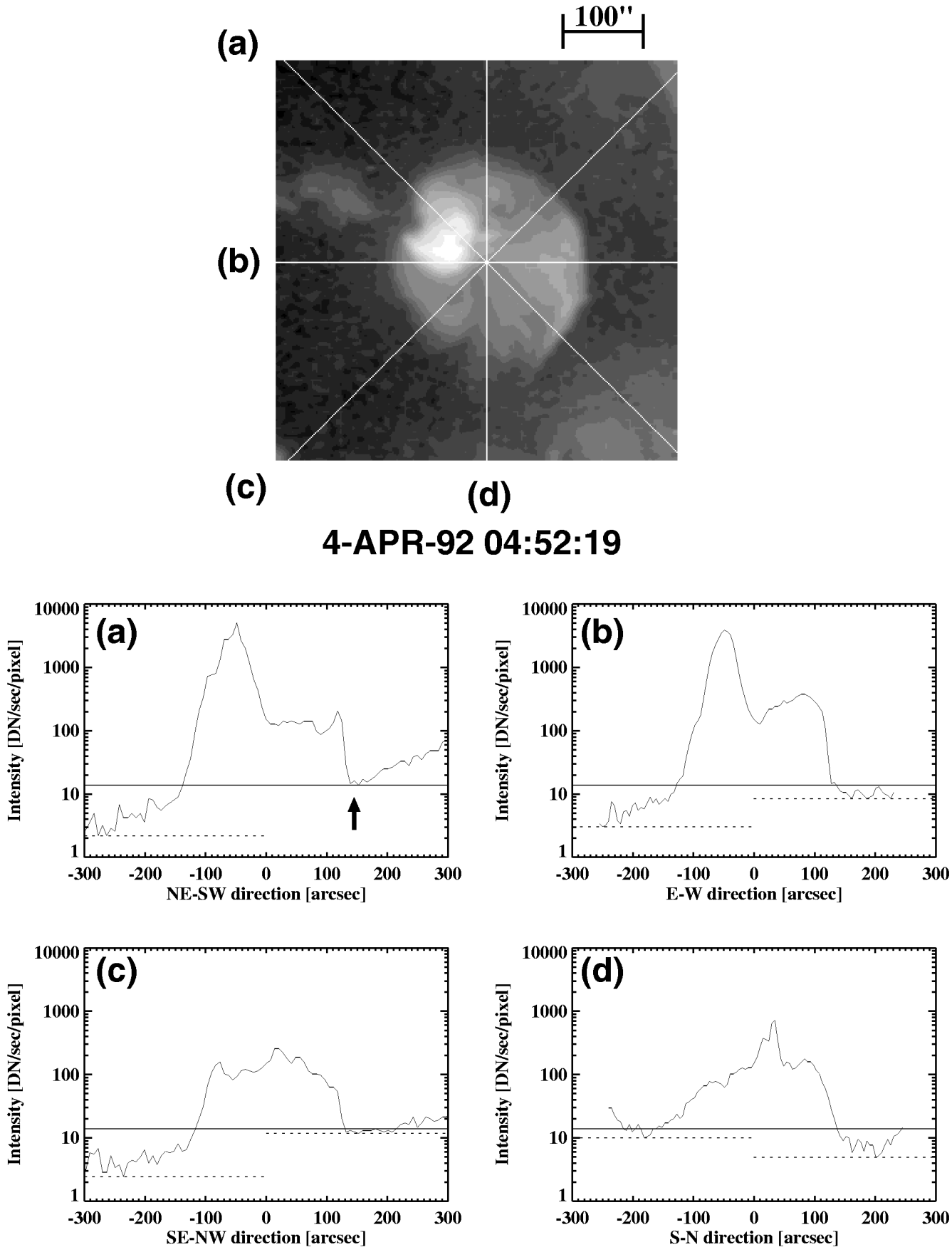

FIG. 2.—Same as Fig. 1, but for the same active region on 1992 April 4 at 04:52:19 UT. In this case, the maximum of minimum values (12 DN s^{-1} $pixel^{-1}$ as indicated by an arrow) is larger than 5 DN s^{-1} $pixel^{-1}$, so that the boundary value (*solid line*) is defined as 12 DN s^{-1} $pixel^{-1}$.

TABLE 1

LIST OF EMERGING FLUX REGIONS

NOAA Number	Birth Date UT (Birth Position)	Velocity of Core Region (km s^{-1})	Velocity of Extended Region (km s^{-1})	Integration Time (hr)	Appearance of AFS (SGD)
7061	1992 Feb 13 (E46, S08)	0.3	0.5	8.46	1992 Feb 14
7090	1992 Mar 3 (E06, N05)	0.3	0.4	10.0	1992 Mar 4
7124	1992 Apr 2 (W08, N13)	0.8	1.2	14.3	1992 Apr 2
7150	1992 Apr 27 (E33, S07)	0.3	1.2	6.06	1992 Apr 28
7400	1993 Jan 10 (E28, S09)	0.5	0.7	6.24	1993 Jan 12
7421	1993 Feb 4 (W43, S12)	0.5	0.4	6.06	1993 Feb 4
7430	1993 Feb 17 (E51, N08)	0.6	1.5	6.50	1993 Feb 17
7466	1993 Mar 30 (E21, S22)	0.8	1.2	7.41	1993 Mar 31
7472	1993 Apr 5 (E14, N04)	0.3	0.4	13.1	1993 Apr 6
7584	1993 Sep 15 (E10, S04)	0.7	0.6	6.35	No AFS
7585	1993 Sep 23 (E25, S08)	1.1	2.6	6.63	1993 Sep 21
7592	1993 Sep 29 (E90, S11)	1.1	1.9	6.44	1993 Oct 1
7601	1993 Oct 15 (E08, N04)	1.6	5.8	6.00	1993 Oct 15
7605	1993 Oct 20 (E16, S17)	1.2	2.6	6.55	1993 Oct 20
7637	1993 Dec 15 (E12, N06)	0.9	1.6	6.48	1993 Dec 15
7658	1994 Jan 19 (E61, N11)	0.2	0.3	8.27	1994 Jan 22
7661	1994 Jan 23 (E59, N07)	0.4	1.1	6.47	1994 Jan 24
7732	1994 Jun 7 (W12, S09)	0.8	1.6	6.09	1994 Jun 7
7733	1994 Jun 8 (E25, N03)	1.4	2.7	6.38	1994 Jun 9
7770	1994 Aug 22 (E60, S08)	0.5	1.0	6.30	1994 Aug 22
7772	1994 Aug 29 (E15, S23)	1.5	2.3	6.19	1994 Aug 29
7848	1995 Feb 27 (E35, S15)	0.7	1.1	6.17	1995 Feb 28
7886	1995 Jun 27 (E60, N11)	0.5	0.7	10.0	1995 Jun 28
7896	1995 Aug 4 (E12, N01)	0.6	0.5	6.07	1995 Aug 5
7900	1995 Aug 15 (W14, N06)	0.8	2.2	6.51	1995 Aug 15
7911	1995 Oct 7 (E28, N07)	2.2	2.6	6.11	1995 Oct 7
7948	1996 Feb 23 (W11, N10)	1.0	1.6	6.50	1996 Feb 23
7953	1996 Mar 21 (E34, N07)	1.4	3.0	6.43	1996 Mar 21
7954	1996 Mar 25 (W09, N02)	1.0	1.6	7.07	1996 Mar 25
7955	1996 Mar 30 (W11, N02)	1.1	1.1	6.07	1996 Apr 1
7956	1996 Apr 11 (E55, N06)	0.6	1.4	7.57	1996 Apr 12
7957	1996 Apr 17 (W34, S09)	0.8	1.7	9.83	1996 Apr 18
7961	1996 May 5 (E19, N13)	1.4	1.9	6.15	1996 May 5

NOTE.—SGD = Solar Geophysical Data.

much lower than that inferred from Hα observations of arch filament systems (Bruzek 1969; Chou & Zirin 1988) as well as from MHD simulation and theory (Shibata et al. 1989). Finally, in § 4, we discuss the early evolution of NOAA 7592, since it is the only example of coronal EFR observed at the limb, thus providing a test of the reliability of our measurement of the apparent expansion velocity. We also discuss some possible ways to account for the discrepancy between Hα observations and our X-ray observations on the expansion velocity of emerging flux.

2. OBSERVATION AND ANALYSIS

All data for this study were obtained using the AlMg filter in the full-frame image (FFI) mode of the *Yohkoh*/SXT. FFI mode images have a spatial resolution of either 5″ (half-resolution) or 10″ (quarter-resolution). This is adequate for resolving EFRs, which are typically of size 30″–40″. Our temporal resolution generally ranges from 10 minutes to an hour, with some exceptions due to occasional large flares or data gaps. Since the duration of EFRs is typically 2–3 days, our temporal resolutions are sufficient for examining the evolution of EFRs. The AlMg filter is sensitive to soft X-rays between 3 and 40 Å and enables observations of plasmas with temperatures from 1.5×10^6 to a few times 10^7 K (Tsuneta et al. 1991). The period during which we track the expansion of ARs is a week or more. In this paper we derive the time evolution of the total X-ray intensity and the region size. In future work we will study the thermal evolution of EFRs using the SXT filter ratio method (Hara et al. 1992).

We chose EFRs which appeared in either coronal holes (CHs) or quiet regions (QRs) because EFRs in these regions have a clear boundary. Consequently, our data set includes many "anemone-type ARs," most of which are active regions (ARs) appearing in CHs and look similar to "sea-anemone" in SXT images (Shibata 1994; Shibata, Nitta, & Hara 1998; Shibata et al. 1996). In the *Skylab* era, these features were called the "fountains" (Sheeley et al. 1975).

We define two subregions for each active region, which we call the *extended region* and the *core region*. The extended region is defined as the portion of the active region with intensity greater than the boundary value. We use the following method to define the boundary value of extended regions.

First, we draw eight straight lines whose lengths are less than 200,000 km from the center of EFRs to the outside. Then we calculate the minimum value of X-ray intensity along these lines. We define the boundary value of X-ray intensity of an EFR as the maximum of minimum values on these lines. If this boundary value is less than 5 DN s^{-1} $pixel^{-1}$ (5″ × 5″), which is roughly equal to the average intensity in coronal holes, we use this critical value (5 DN s^{-1} $pixel^{-1}$) for the boundary value. Figure 1 shows an example of our definition of an extended region in the early phase of an active region NOAA 7124. The solid curves in the figures in the middle and lower panels show the X-ray

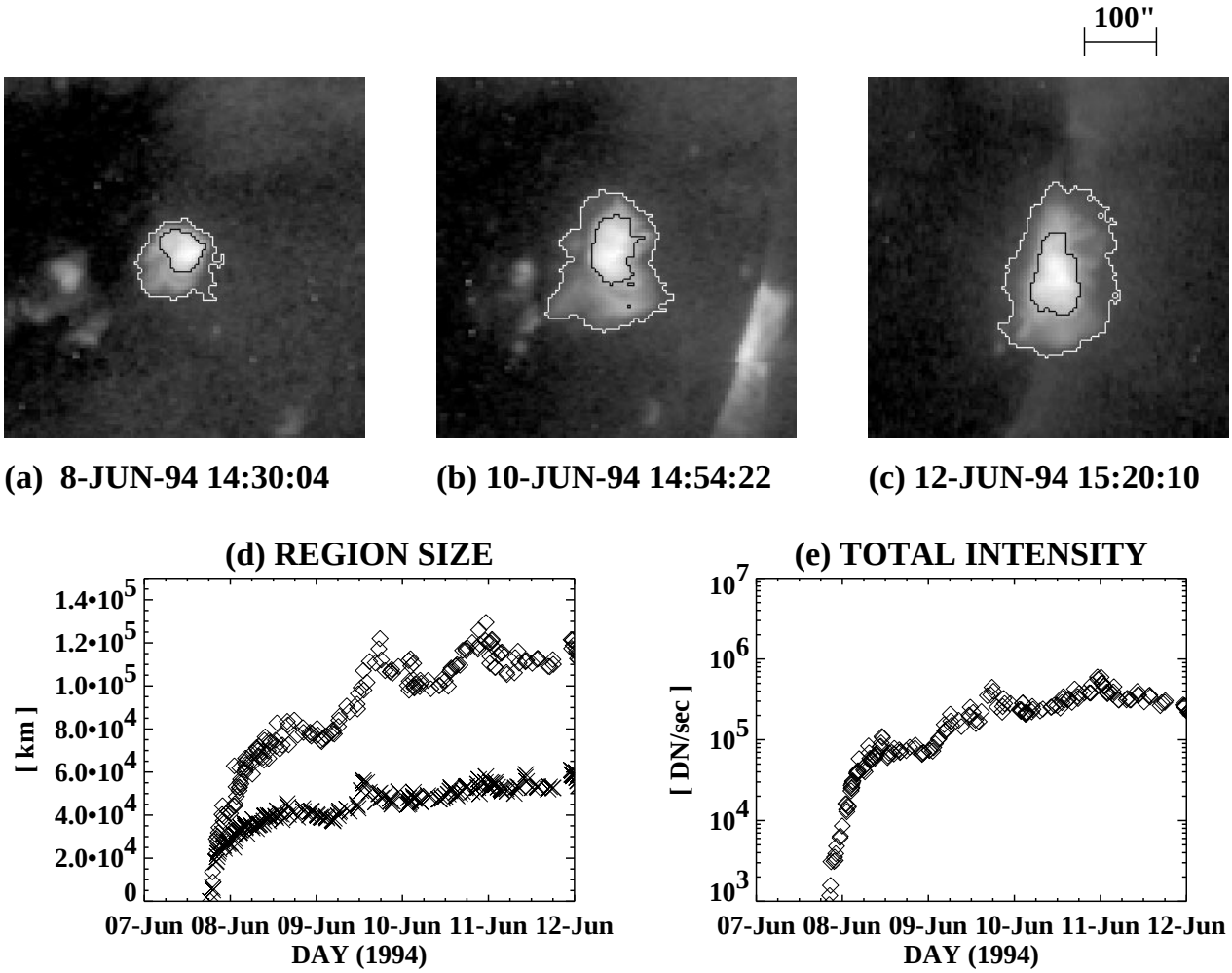

FIG. 5.—Time developments of core/extended region (NOAA 7732). (*a–c*) Boundaries of core region (*black curve*) and extended region (*white curve*) are shown. (*d*) Time evolution of the region size for core region (*crosses*) and extended region (*diamonds*). (*e*) Time evolution of the total soft X-ray intensity of extended region.

intensity distribution along each line. The dashed lines correspond to the minimum value of the intensity in each line. Since the maximum among these minimum values (indicated by an arrow) is less than 5 DN s^{-1} $pixel^{-1}$ in this case, the boundary value of X-ray intensity of the active region is defined as 5 DN s^{-1} $pixel^{-1}$. On the other hand, in the case of Figure 2, the maximum of minimum values on straight lines (about 12 DN s^{-1} $pixel^{-1}$) is larger than 5 DN s^{-1} $pixel^{-1}$, and hence this value is adopted as the boundary value of the X-ray intensity of the active region.

We define the core region as the portion of the active region radiating the brightest 80% of the total integrated soft X-ray intensity of the EFR. (In some cases a core region consists of two or more subregions inside the EFR.)[4] The motivation of our definition of the core region and the extended region is not to examine the structure of the EFR in detail but simply to demonstrate the generality of our results using two different subregions when deriving the size and the expansion velocity of the EFR. This is because it is difficult to define the boundary of the active regions. In fact, as seen later, the patterns of evolution of the size of both core region and extended region are similar, and even the apparent expansion velocities are not so different within a factor of 2 between both regions (Table 1). Nevertheless, it is interesting to note that the core region seems to correspond to the magnetic loops directly emerged from below, whereas the extended region contains the region connected by magnetic reconnection between emerging flux and ambient flux (see also Kitt Peak magnetograms in Fig. 4).

We define the size of an EFR as the square root of the area of either the extended region or the core region, and derive the apparent velocity of expansion of an EFR from the time variation of its size. In deriving the size of an EFR, we do not take into account projection effects, because we cannot determine the height of an EFR. Let us estimate the error in the size of an EFR due to projection effects. If coronal EFRs have a plane structure parallel to the solar surface, the error in size due to projection effects is less than 55% except for one case which is observed just at the limb. Our deduced velocities tend to be lower than the true values with a possible maximum error of 55%, because the former are derived from the projected area. However, actual EFRs do not have a plane structure but have a three-dimensional

[4] We also analyzed the temperature distribution in EFRs, and found that we cannot see a clear boundary of the EFRs in temperature maps if we retain a temporal resolution of 30–90 minutes using FFI data. Emission measure maps are found to be nearly the same as the intensity maps.

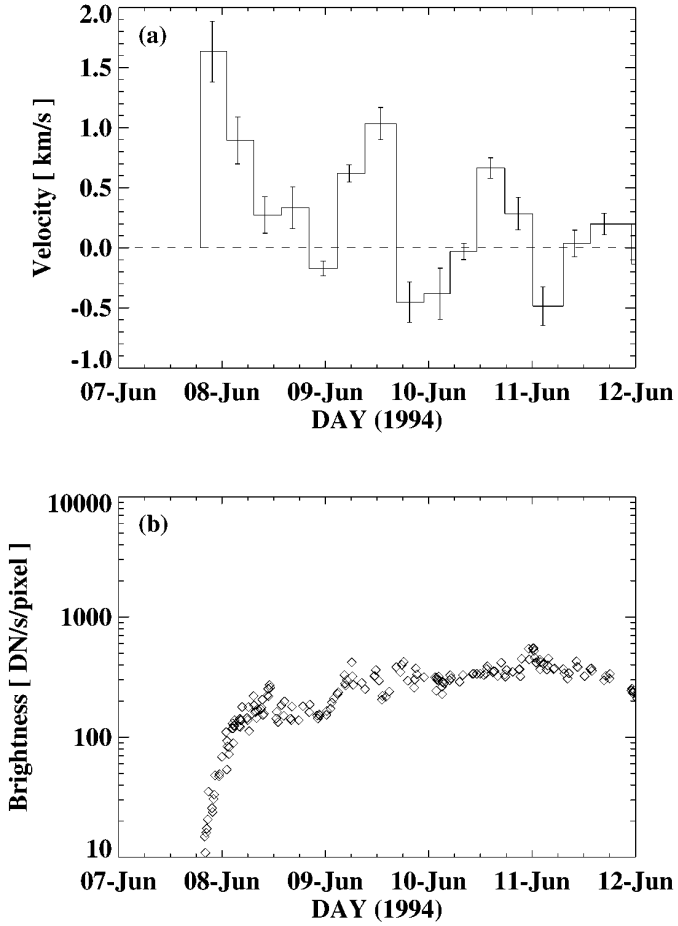

FIG. 6.—(*a*) Time variation of the apparent velocity of the expansion of the EFR NOAA 7732. (*b*) Surface brightness (I_{total}/A) for the EFR NOAA 7732, where I_{total} is the total soft X-ray intensity of the extended region.

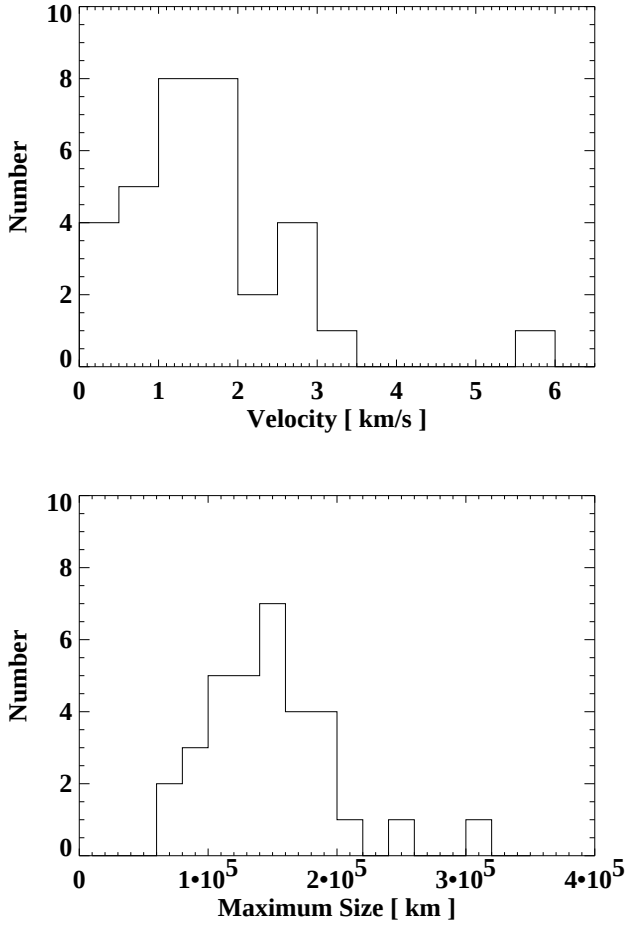

FIG. 7.—Histograms of the initial expansion velocity of the extended region and the maximum region size.

structure (more like a hemisphere than a plane), as shown in the case of EFRs observed near the limb (e.g., see Fig. 8), so that the projection effect is actually not important.

3. RESULTS

We analyze 33 emerging flux regions that appeared in coronal holes or quiet regions and examine the time variation of the region size and the total X-ray intensity. Figure 3 (Plate 49) shows the time series of SXT images of a typical active region (NOAA 7732), revealing the rapid growth in size of the region during the early phase of the evolution. AR 7732 had not yet appeared at 18:24 UT on 1994 June 7, but had already appeared at 20:21 UT on 1994 June 7. At this stage, the size of the AR is ~21,000 km. The AR grows to ~42,000 km at 23:59 UT on 1994 June 7. Hence, the average expansion velocity between 20:21 UT and 23:59 UT is ~1.6 km s^{-1}. Figure 4 (Plate 50) shows the comparison of SXT images of the AR 7732 with the nearly simultaneous Kitt Peak magnetograms, which are coaligned with SXT images, revealing that the compact bright structure in SXT images corresponds to magnetic bipoles. Detailed comparison between *Yohkoh* SXT images and Kitt Peak magnetograms has revealed that when the magnetic bipole appears, the soft X-ray bright loop (or bright points) appear. Whether this is really the emerging flux or not is easily checked by observing the later evolution of the same region. Hence *we define coronal EFRs as X-ray bright loops/points associated with a magnetic bipole that will eventually evolve into the normal active regions.* Note that the Kitt Peak magnetogram is a daily image, and hence we often cannot check whether there is really a magnetic bipole associated with the first image of the X-ray bright loops/points. In this sense, the error of the time of the first appearance of a coronal EFR is a few hours (average time difference between the first coronal EFR images and Kitt Peak magnetograms).

Figures 5*a*–5*c* show the boundaries of the extended region (*white*) and of the core region (*black*). We measure the projected area, A, of the extended region and the core region, and define the "region size," L, of these regions as $L = A^{1/2}$.

We derive the apparent velocity of expansion of the extended region and the core region from the time variation of L. Figure 6 shows the time variation of the expansion velocity of EFR 7732. Here the velocity is defined as the slope of the least-squares–fitting straight line on the time-variation curve of L over 6 hr.

In the case of EFR 7732, the expansion velocity is largest (~1.6 km s^{-1}) in the initial phase ($t < 6$ hr after the birth of the region), and becomes less than 1 km s^{-1} in a later phase. The expansion velocity increases again to ~1 km s^{-1} on 1994 June 9, followed by a sudden decrease. It seems that the expansion velocity decreases with time but with some occasional increase corresponding to intermittent fast expansion of the EFR. The time evolution of

the surface brightness ($=I_{\rm total}/A$) of these regions is also shown in Figure 6, where $I_{\rm total}$ is the total soft X-ray intensity of the extended region. Interestingly, the velocity seems to be correlated with the surface brightness.

Table 1 summarizes the results of analysis of 33 EFRs. We find that the initial apparent velocities of the core regions are 0.2–2.2 km s^{-1}, whereas those of the extended regions are 0.3–5.8 km s^{-1} (see Table 1). Here the initial velocity is estimated during 6 hr after the first X-ray image of each EFR. Figure 7 shows the distribution of the initial expansion velocity of the extended region. We find that most of the initial velocities are less than 2 km s^{-1}.

4. DISCUSSION

We found that the apparent expansion velocity of EFRs (core/extended region) is relatively large (0.2–5.8 km s^{-1}) during the very early phase of the EFR evolution. This result partly confirms the results of preliminary studies by Ishido et al. (1992) and Su et al. (1995), who found the initial velocity of EFRs to be of the order of a few kilometers per second. It is interesting to note that the initial velocity is comparable to the separation velocity of the two footpoints of emerging flux (Harvey & Martin 1973; Chou 1993).

The apparent rise velocity is about half the expansion velocity because the apparent shape of EFRs is roughly hemispherical. Hence, the rise velocity is less than 1.0 km s^{-1}. This is much slower than the rise velocity of Hα arch filaments ($\sim$10–20 km s^{-1}). Two-dimensional MHD numerical simulation and theory of Shibata et al. (1989, 1990) also predict a fast rise velocity for EFR loops ($\sim$10–20 km s^{-1}). (See also Nozawa et al. 1992 for an extensive parameter survey in the two-dimensional model and Matsumoto et al. 1993 for three-dimensional MHD simulations.) What is the cause of the discrepancy between Hα observations and X-ray observations?

In this regard, we show one interesting case (in FFI data) that reveals the early evolution of a coronal EFR at the limb (NOAA 7592; see Fig. 8 [Pl. 51]) at a relatively better time cadence (10–30 minutes except for an occasional data gap). Figure 9*a* depicts the time variation of the size of this coronal EFR, showing that the apparent expansion velocity of the coronal EFR is 3–5 km s^{-1} in the very early stage (less than 3 hours after birth), even though it is about 0.9–1.5 km s^{-1} on average in the longer period (less than 34 hours after birth). The latter is comparable to the expansion velocities of other EFRs (Table 1). It is interesting to note that the region size shows intermittent fast expansion above 3 km s^{-1} (at 10 UT and 23 UT on September 29, and at 7 UT on September 30). This seems to be similar to the episodic expansion observed in NOAA 7732 (Figs. 3 and 4), although the time interval of fast expansions is shorter in NOAA 7592. Similar intermittent fast expansion of active region corona is also observed in well-developed active regions (e.g., Uchida et al. 1992; Wang et al. 1997). There are two points we can learn from this particular case: (1) The younger the EFR, the larger the expansion velocity of the coronal EFR. (2) Nevertheless, the expansion velocity is still smaller than that of AFSs. In this particular case, we can examine vertical expansion of the coronal EFR, since the EFR appeared at the limb. Figure 9*b* compares the time variations of height and horizontal size of this EFR, confirming that the vertical expansion velocity is comparable to the horizontal expansion velocity, as expected from the shape of the other coronal EFRs. Unfortunately, this is the only limb observation of coronal EFRs with such good quality until now.

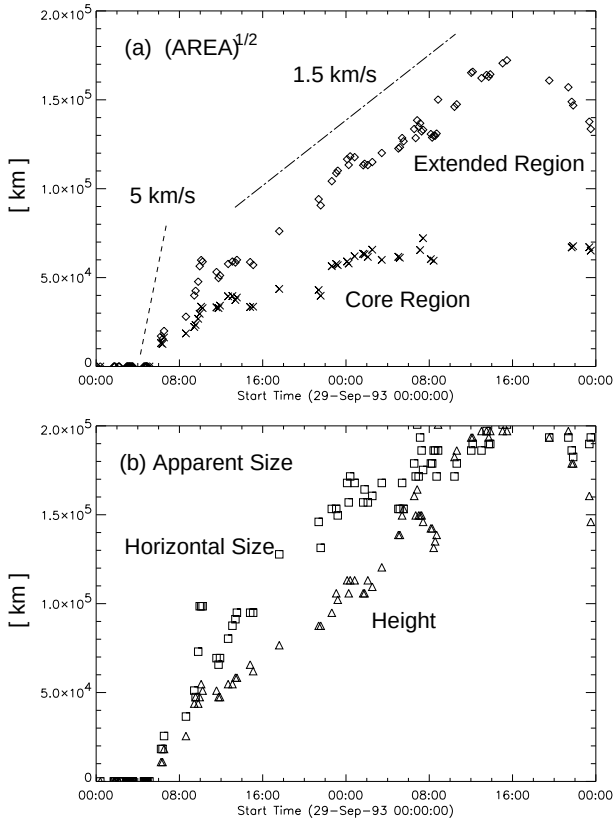

FIG. 9.—Time variation of the size of NOAA 7592 observed at the limb. (*a*) Region size defined by $A^{1/2}$, where A is the projected area of the coronal EFR; values for the extended region are shown by diamonds, and those for the core region by crosses. (*b*) Apparent sizes of the EFR, which are measured using the boundary contours of the extended region; the horizontal size is shown by squares, and the height by triangles. Note that the apparent expansion velocity in the very early phase (less than 3 hours after birth) is very large ($\sim$3–5 km s^{-1}).

Let us now consider the cause of the discrepancy between the expansion velocities of coronal EFRs found by soft X-ray observations and those inferred from Hα observations and MHD simulation and theory. One possibility is that the rise velocity of the emerging magnetic flux may have slowed down during a very early phase of its evolution (less than 10–30 minutes, which is the time resolution in FFI mode). In that case, the slow expansion velocity of coronal emerging loops might simply be a manifestation of slow footpoint motion of emerging magnetic loops. To check this, it is necessary to measure the velocity of EFRs during the very early phase (i.e., before coronal emerging flux settles in a quasi-magnetostatic state). If *Yohkoh*/SXT observes EFRs in partial frame image (PFI) mode from the very beginning of their birth, it would be possible to detect such high-velocity EFR expansion ($\sim$10 km s^{-1}) if it exists. In PFI mode, the SXT's spatial resolution is 2.″5 (full resolution), and its time resolution is about 1 minute.

The other possibility is that the apparent expansion of EFRs in soft X-rays does not reflect the actual rise motion of magnetic loops. That is, magnetic loops might be actually moving upward at $\sim$10–20 km s^{-1}, but this motion may not be visible in SXT images. In fact, listings in Solar Geophysical Data (SGD) (in the last column in Table 1), indicate that in many EFRs, arch filament systems appear

nearly simultaneously with, or later than, the X-ray emerging flux. This means that fast rise motions ($\sim$10–20 km s^{-1}) of emerging loops must be present at least just above Hα emerging loops, at times when the "apparent" velocity of X-ray EFRs has decreased to less than 0.5 km s^{-1}. In order to detect such fast rise motions just above Hα emerging loops, we require Doppler shift measurements of coronal plasmas, which may be possible with the *SOHO* spacecraft and/or the next Japanese solar mission (*Solar B*).

The authors would like to thank all of the *Yohkoh* team members, and also thank A. Sterling and S. Savy for useful comments. The *Yohkoh* satellite is a Japanese national project, launched and operated by ISAS, and involving many domestic institutions, with multilateral international collaboration with the US and the UK. The NSO/Kitt Peak data used here are produced cooperatively by NSF/NOAO, NASA/GSFC, and SEC/NOAA.

REFERENCES

Bruzek, A. 1967, Sol. Phys., 2, 451
———. 1969, Sol. Phys., 8, 29
Chou, D., & Zirin, H. 1988, ApJ, 333, 420
Chou, D. Y. 1993, in ASP Conf. Ser. 46, The Magnetic and Velocity Field of Solar Active Regions, ed. H. Zirin, G. Ai, & H. Wang (San Francisco: ASP), 471
Gaizauskas, V. 1993, Adv. Space Res., 13(9), 5
Hara, H., Tsuneta, S., Lemen, J. R., Acton, L. W., & McTiernan, J. M. 1992, PASJ, 44, L135
Harvey, K. L., & Martin, S. F. 1973, Sol. Phys., 32, 389
Ishido, Y., Shibata, K., Tanaka, N., & Kurokawa, H. 1992, in Proc. Conf. on Study of Solar Active Phenomena Induced by Magnetic Shear: New Results of *Yohkoh* Observations (Tokyo: Natl. Astron. Obs.), 145
Kawai, G., Kurokawa, H., Tsuneta, S., Shimuzu, T., Shibata, K., Acton, L. W., Strong, K. T., & Nitta, N. 1992, PASJ, 44, L193
Kurokawa, H. 1988, in Proc. Fourth Asian-Pacific Regional Meeting of the IAU (Vistas Astron., Vol. 31), 67
Marsh, K. A. 1978, Sol. Phys., 59, 105
Matsumoto, R., Tajima, T., Shibata, K., & Kaisig, M. 1993, ApJ, 414, 357
Nozawa, S., Shibata, K., Matsumoto, R., Sterling, A., Tajima, T., Uchida, Y., Ferrari, A., & Rosner, R. 1992, ApJS,78, 267
Ogawara, Y., Takano, T., Kosugi, T., Tsuneta, S., Watanabe, T., Kondo, I., & Uchida, Y. 1991 Sol. Phys., 136, 1
Parker, E. N. 1979, Cosmical Magnetic Field (Oxford: Oxford Univ. Press)
Sheeley, N. R., Jr., Bohlin, J. D., Bruechner, G. E., Purcell, J. D., Scherrer, V., & Tousey, R. 1975, Sol. Phys., 40, 103
Shibata, K. 1994, in IAU Colloq. 143, The Sun as a Variable Star: Solar and Stellar Irradiance Variations, ed. J. M. Pap, C. Fröhlich, H. S. Hudson, & S. K. Solanki (Cambridge: Cambridge Univ. Press), 89
Shibata, K., Nitta, N. & Hara, H. 1998, in preparation
Shibata, K., Nozawa, S., Matsumoto, R., Sterling, A., & Tajima, T. 1990, ApJ, 351, L25
Shibata, K., Tajima, T., Steinolfson, R., & Matsumoto, R. 1989, ApJ, 345, 584
Shibata, K., Yokoyama, T., & Shimojo, M. 1996, J. Geomagn. Geoelectr., 48, 19
Shimizu, T., Tsuneta, S., Title, A., Tarbell, T., Shine, R., & Frank, Z. 1996, in IAU Colloq. 153, Magnetodynamic Phenomena in the Solar Atmosphere: Prototype of Stellar Magnetic Activity, ed. Y. Uchida et al. (Dordrecht: Kluwer), 37
Shimojo, M., Hashimoto, S., Shibata, K., Hirayama, T., Hudson, H. S., & Acton, L. W. 1996, PASJ, 48, 123
Su, Q., Hirayama, T., Shibata, K., Ichimoto, K., Tsuneta, S., Hara, T., Acton, L. & Lemen, J. 1995, in Proc. Third China-Japan Seminar on Solar Physics, ed. J. Wang et al. (Beijing: Int. Acad. Publishers), 47
Tsuneta, S., et al. 1991, Sol. Phys., 13, 37
Uchida, Y., McAllister, A., Strong, K. T., Ogawara, Y., Shimizu, T., Matsumoto, R., & Hudson, H. S. 1992, PASJ, 44, L155
Wang, J., Shibata, K., Nitta, N., Slater, G. S., Savy, S. K., & Ogawara, Y. 1997, ApJ, 478, L41
Webb, D. F. 1981, in Proc. *Skylab* Workshop on Solar Active Region, ed. F. Q. Orrall (Boulder: Univ. Colorado Press), 165
Yokoyama, T., & Shibata, K. 1995, Nature, 375, 42
———. 1996, PASJ, 48, 353
Zirin, H. 1972, Sol. Phys., 22, 34
———. 1988, Astrophysics of the Sun (Cambridge: Cambridge Univ. Press), 321
Zwaan, C. 1987, ARA&A, 22, 34

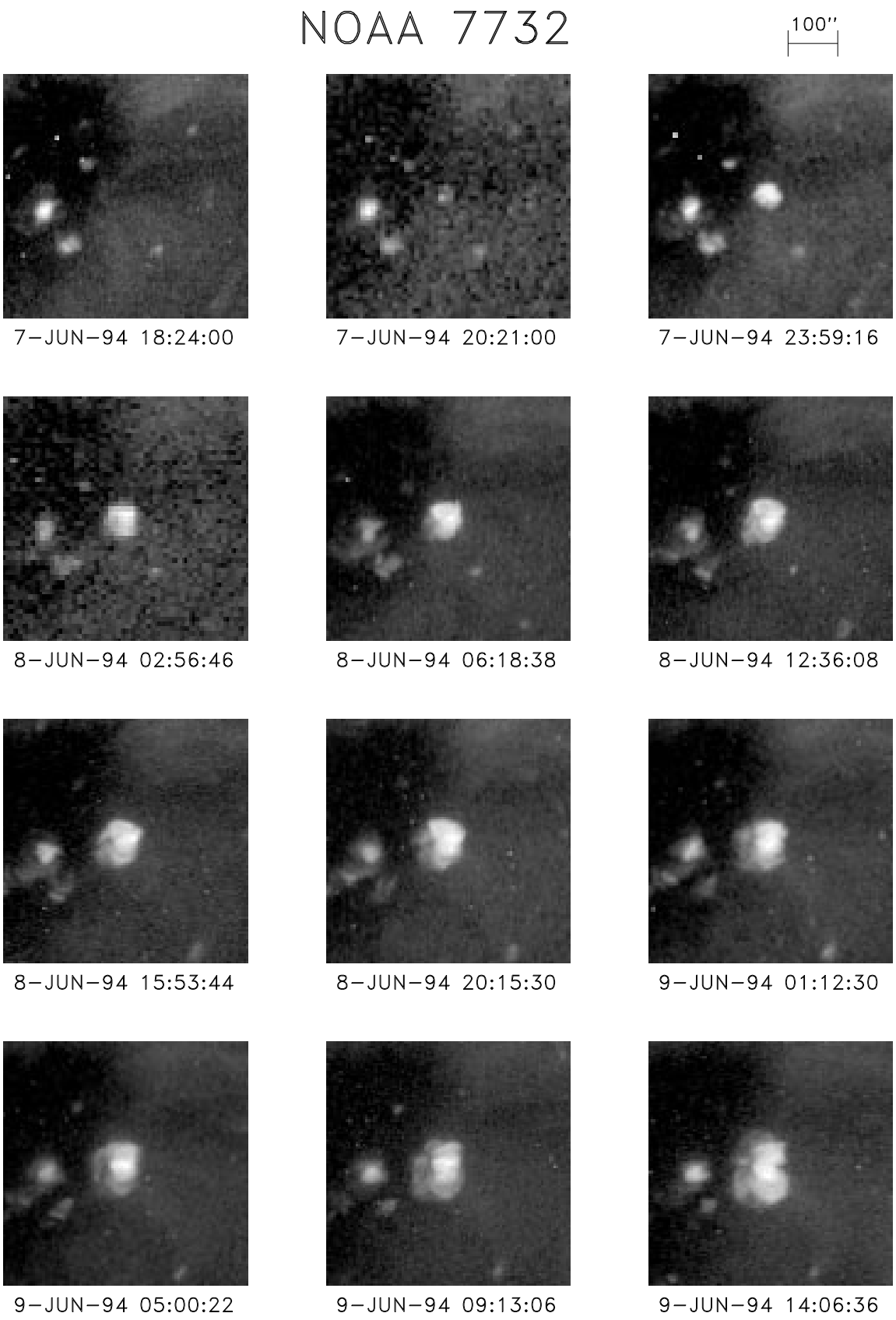

FIG. 3.—Time evolution of coronal emerging flux region. The SXR images were taken with the SXT AlMg filter at half-resolution (5″) or quarter-resolution (10″); 100″ corresponds to 73,000 km.

YASHIRO, SHIBATA, & SHIMOJO (see 493, 975)

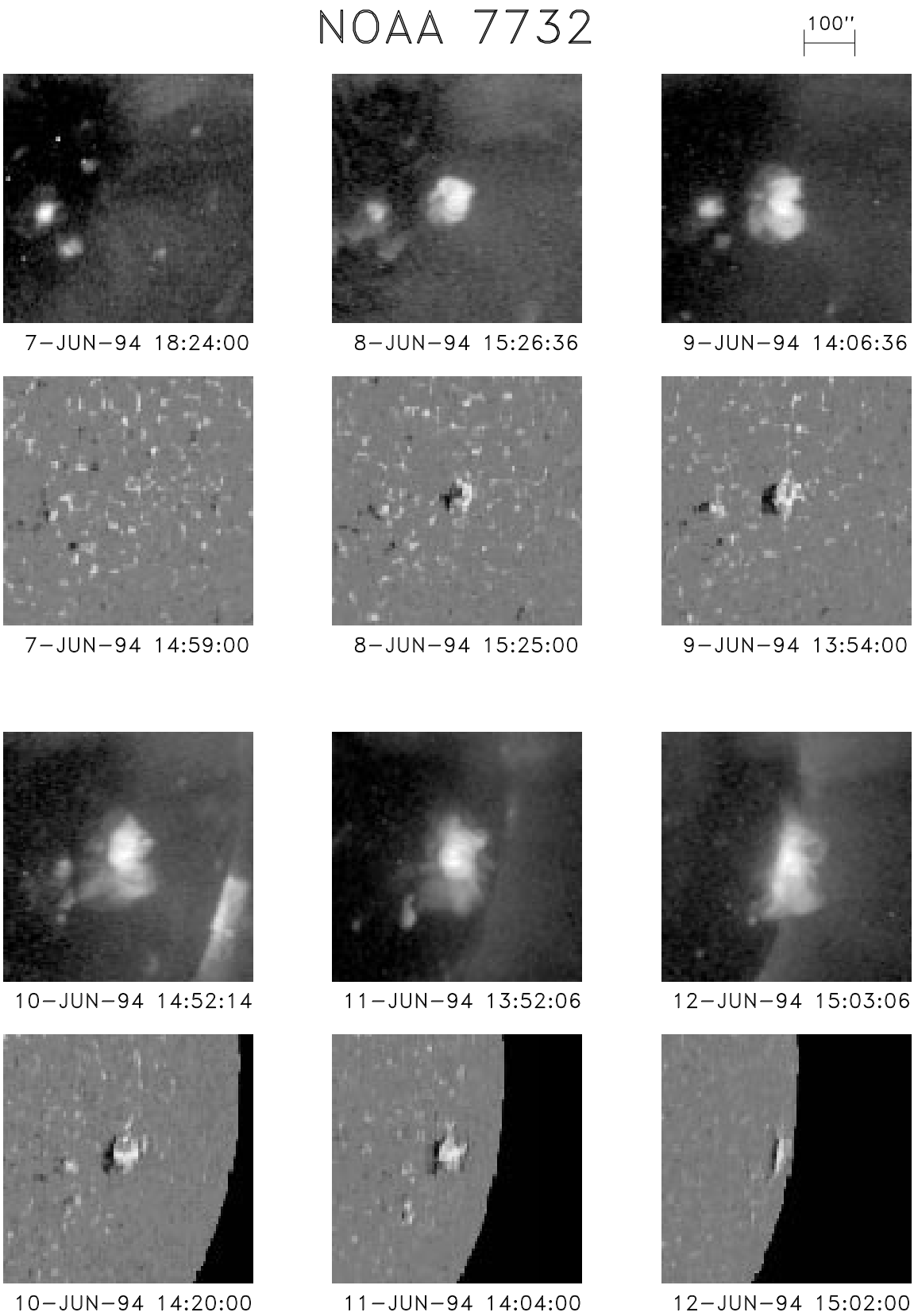

FIG. 4.—Time evolution of emerging flux region. These panels show daily soft X-ray images of NOAA 7732 and the nearly simultaneous Kitt Peak magnetograms. The SXR images were taken with the SXT AlMg filter at half-resolution (5″) or quarter-resolution (10″); 100″ corresponds to 73,000 km.

YASHIRO, SHIBATA, & SHIMOJO (see 493, 975)

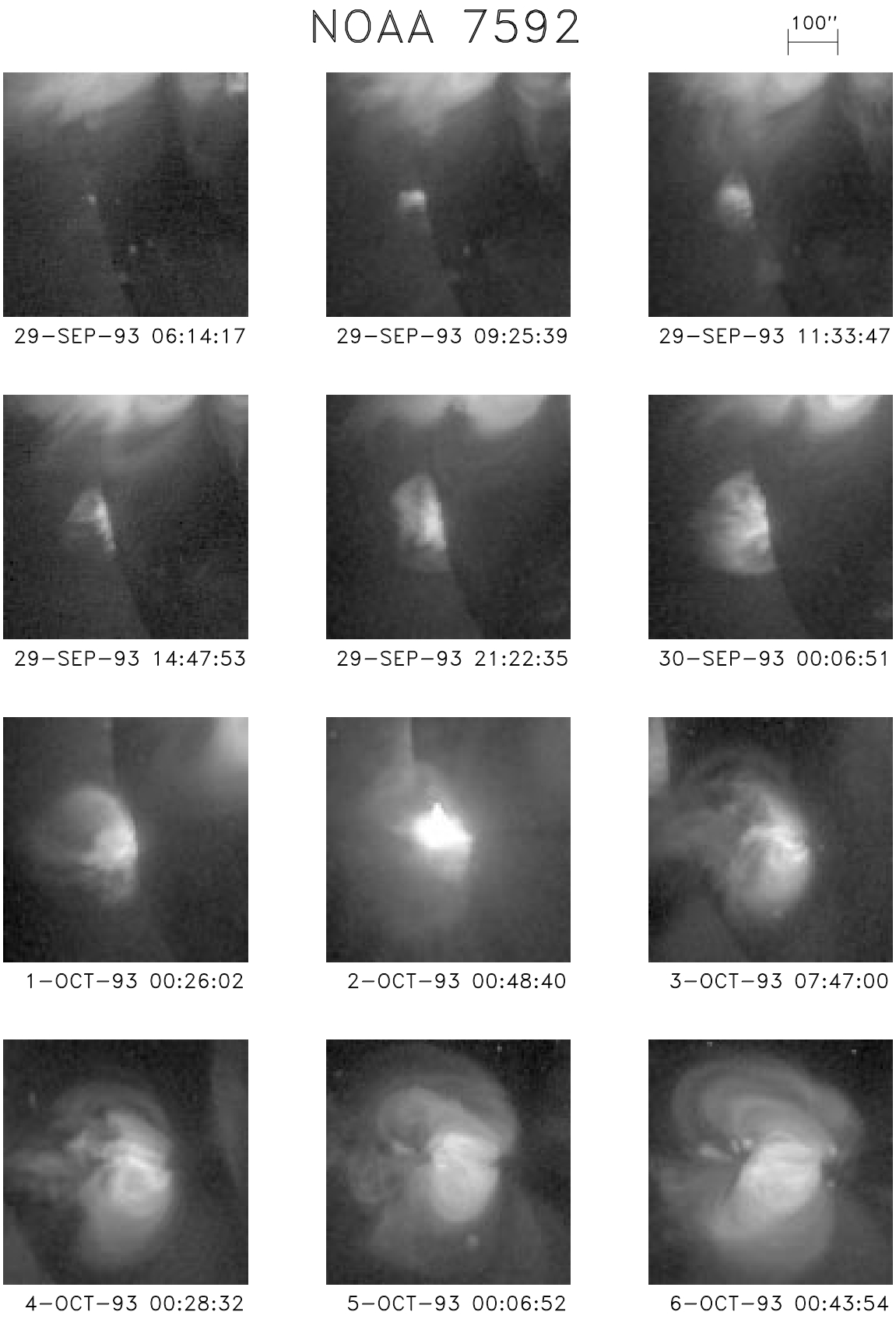

FIG. 8.—Coronal EFR observed at the limb. Time series of soft X-ray images of NOAA 7592. The upper panels show the early stage of evolution.

YASHIRO, SHIBATA, & SHIMOJO (see 493, 976)

PLATE 51